Supporting Information

Size-dependent electron transfer from atomically defined nanographenes to metal oxide nanoparticles

Peng Han[1], Xuelin Yao[1], Klaus Müllen[1,2], Akimitsu Narita[1,3], Mischa Bonn[1], Enrique Cánovas[1,4,*]

[1] Max Planck Institute for Polymer Research, Ackermannweg 10, 55128 Mainz, Germany.

[2] Institute of Physical Chemistry, Johannes Gutenberg University Mainz, Duesbergweg 10-14, 55128 Mainz, Germany.

[3] Organic and Carbon Nanomaterials Unit, Okinawa Institute of Science and Technology Graduate University, Okinawa 904-0495, Japan.

[4] Instituto Madrileño de Estudios Avanzados en Nanociencia (IMDEA Nanociencia), Faraday 9, 28049 Madrid, Spain.

** Correspondence to: enrique.canovas@imdea.org*

SAMPLE PREPARATION

General information

All commercially available chemicals were used without further purification unless otherwise noted. Column chromatography was conducted with silica gel (grain size 0.04–0.063 mm) and thin layer chromatography (TLC) was performed on silica gel-coated aluminum sheets with F254 indicator. Nuclear magnetic resonance (NMR) spectra were recorded on Bruker Avance 300 or 500 MHz spectrometer. Chemical shifts were reported in ppm. Coupling constants (*J* values) were presented in Hertz (Hz). ^{1}H NMR chemical shifts were referenced to CD_2Cl_2 (5.32 ppm) or $C_2D_2Cl_4$ (6.00 ppm). ^{13}C NMR chemical shifts were referenced to CD_2Cl_2 (53.84 ppm) or $C_2D_2Cl_4$ (73.78 ppm). Abbreviations: s = singlet, d = doublet, m = multiplet. High-resolution mass spectrometry (HRMS) was performed on a SYNAPT G2 Si high resolution time-of-flight (TOF) mass spectrometer (Waters Corp., Manchester, UK) by matrix-assisted laser desorption/ionization (MALDI). Melting points were measured with a Büchi B-545 apparatus. Absorption spectra were recorded on a Perkin-Elmer Lambda 900 spectrophotometer. DFT calculations were performed using the Gaussian 09 software package [1]. The geometries were optimized at the B3LYP/6-31G(d, p) level, and energies were calculated at the same level of theory. 3,4-Bis[4-(*tert*-butyl)phenyl]-2,5-diphenylcyclopenta-2,4-dien-1-one (**6**) was synthesized according to reported procedures [2].

Scheme S1. Synthesis of nanographene C78 / 27 with *tert*-butyl groups.

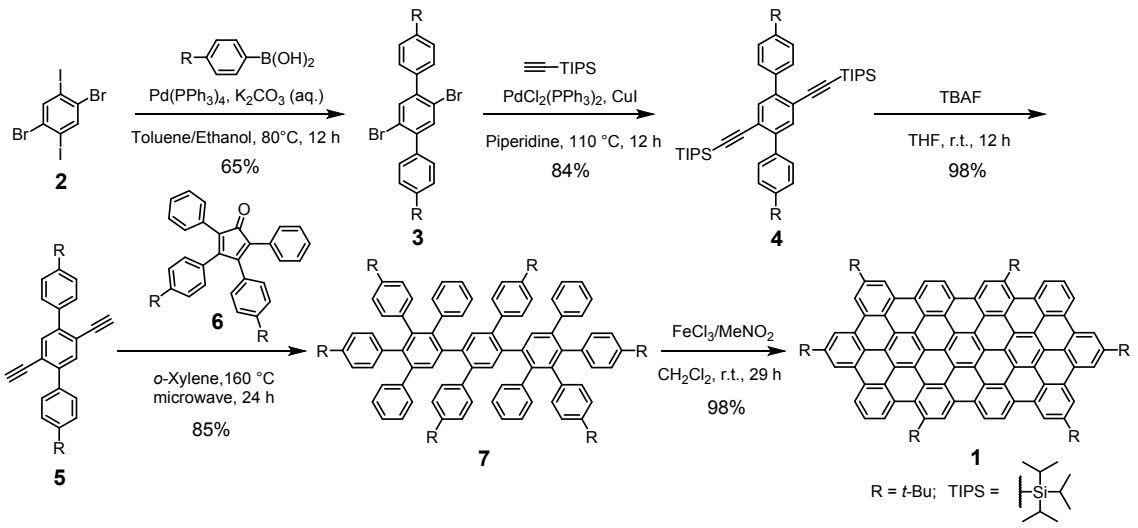

The synthesis of nanographene **1** (C78 / 27) was carried out as displayed in Scheme S1. Suzuki-Miyaura coupling of 1,4-dibromo-2,5-diiodobenzene (**2**) with 4-*tert*-butylphenylboronic acid gave 2',5'-dibromo-4,4''-di-*tert*-butyl-1,1':4',1''-terphenyl (**3**), followed by Sonogashira coupling with triisopropylsilylacetylene to provide 4,4’’-di-*tert*-butyl-2’,5’-di(triisopropylsilylethynyl)-*p*-terphenyl (**4**). Subsequently, **4** was deprotected by treatment with tetra-*n*-butylammonium fluoride to afford 4,4’’-di-*tert*-butyl-2’,5’-diethynyl-*p*-terphenyl (**5**), which was subjected to Diels–Alder reaction with tetraphenylcyclopentadienone **6** to afford oligophenylene precursor **7**. Finally, cyclodehydrogenation reaction of **7** with iron (III) chloride provided nanographene **1**.

Synthesis of 2',5'-dibromo-4,4''-di-*tert*-butyl-1,1':4',1''-terphenyl (3)

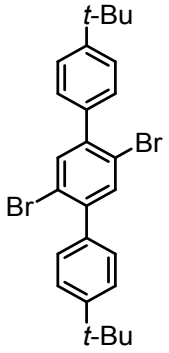

To a two-necked Schlenk flask charged with 1,4-dibromo-2,5-diiodobenzene (**2**) (3.00 g, 6.15 mmol), 4-*tert*-butylphenylboronic acid (2.74 g, 15.4 mmol), and tetrakis(triphenylphosphine)palladium(0) (355 mg, 0.307 mmol) was added degassed toluene (60 mL), a degassed aqueous solution of potassium carbonate (18.5 mL, 2 M), and degassed ethanol (18.5 mL) under argon. The reaction mixture was stirred at 80 °C for 12 h. After cooling to room temperature, the mixture was extracted with dichloromethane (three times) and washed with water. Then the combined organic phases were dried over anhydrous magnesium sulfate. After removal of the solvent under reduced pressure, the residue was purified by column chromatography over silica gel (eluent: hexane : dichloromethane = 15 : 1) to afford compound **3** as white solid (2.00 g, 65% yield). M.p.: 258.6 – 260.2 °C. ^{1}H NMR (300 MHz, CD_2Cl_2, 298 K, ppm) δ 7.65 (s, 2H), 7.50 (d, J = 8.4 Hz, 4H), 7.40 (d, J = 8.4 Hz, 4H), 1.38 (s, 18H); ^{13}C NMR (75 MHz, CD_2Cl_2, 298 K, ppm) δ 151.65, 142.99, 136.93, 135.73, 129.36, 125.52, 121.67, 34.99, 31.48; HRMS (MALDI-TOF, positive) m/z: Calcd for $C_{26}H_{28}Br_2$: 498.0558; Found: 498.0596 $[M]^+$.

Synthesis of 4,4''-di-*tert*-butyl-2',5'-di(triisopropylsilylethinyl)-*p*-terphenyl (4)

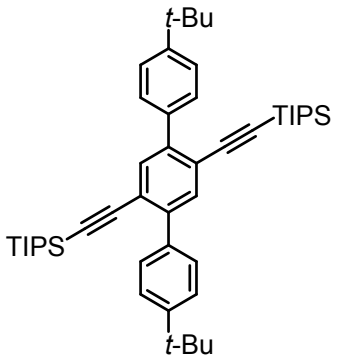

Compound **3** (1.85 g, 3.70 mmol), copper(I)iodide (70.5 mg, 0.370 mmol), and bis(triphenylphosphane)palladium(II) dichloride (260 mg, 0.370 mmol) were dissolved in piperidine (30 mL) under argon atmosphere. Triisopropylsilylacetylene (1.69 g, 9.25 mmol) was

added and the reaction mixture was stirred at 110 °C for 12 h. After cooling to room temperature, the reaction mixture was poured into hydrochloric acid (150 mL, 6 M) followed by extracted with dichloromethane (three times). The combined organic phases were washed with saturated ammonium chloride solution and water, and dried over anhydrous magnesium sulfate. After evaporating the solvent, the crude product was purified by column chromatography over silica gel (eluent: hexane : dichloromethane = 10 : 1) to afford compound **4** (2.18 g, 84% yield) as white solid. M.p.: 271.6 – 272.5 °C. ^{1}H NMR (300 MHz, CD_2Cl_2, 298 K, ppm) δ 7.60 – 7.52 (m, 6H), 7.48 – 7.41 (m, 4H), 1.39 – 1.31 (s, 18H), 1.06 – 0.97 (m, 42H); ^{13}C NMR (75 MHz, CD_2Cl_2, 298 K, ppm) δ 150.99, 143.02, 136.90, 134.57, 129.26, 125.40, 122.41, 106.44, 96.17, 34.86, 31.48, 18.76, 11.70; HRMS (MALDI-TOF, positive) *m*/*z*: Calcd for $C_{48}H_{70}Si_2$: 702.5016; Found: 702.5047 $[M]^+$.

Synthesis of 4,4''-di-*tert*-butyl-2',5'-diethinyl-*p*-terphenyl (5)

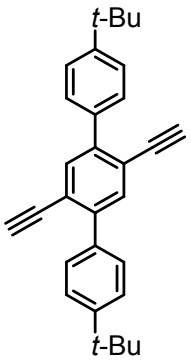

Tetra-*n*-butylammonium fluoride (TBAF) (3.24 g, 12.4 mmol) was added to compound **4** (2.18 g, 3.10 mmol) dissolved in tetrahydrofuran (40 mL). After stirring at room temperature for 12 h, the reaction mixture was poured into water and extracted with dichloromethane for three times. The combined organic phases were then washed with water and dried over anhydrous magnesium sulfate. After evaporating the solvent, the crude product was purified by column chromatography over silica gel (eluent: hexane : dichloromethane = 5 : 1) to afford compound **5**

(1.19 g, 98% yield) as a white solid. M.p.: 252.9 – 253.9 °C. ^{1}H NMR (300 MHz, CD_2Cl_2, 298 K, ppm) δ 7.68 (s, 2H), 7.62 (d, J = 8.2 Hz, 4H), 7.48 (d, J = 8.2 Hz, 4H), 3.25 (s, 2H), 1.39 (s, 18H); ^{13}C NMR (75 MHz, CD_2Cl_2, 298 K, ppm) δ 150.78, 141.93, 135.35, 135.08, 128.63, 125.01, 120.55, 82.92, 81.98, 34.44, 31.25; MS (MALDI-TOF, positive) *m*/*z*: Calcd for $C_{30}H_{30}$: 390.2348; Found: 390.2474 $[M]^+$.

Synthesis of 2'',3''',4''',5',5'',6'-hexakis(4-*tert*-butylphenyl)-1,1':2',1'':4'',1''':2''',1''''-quinquephenylene (7)

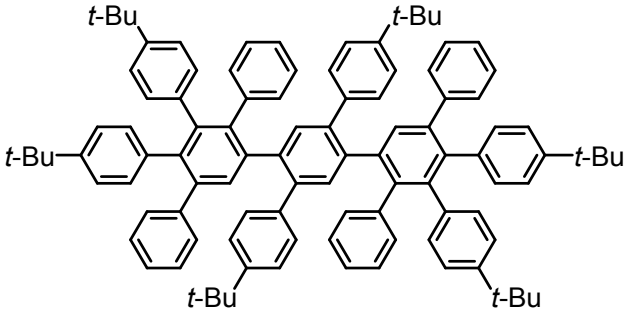

To a microwave vessel charged with compound **5** (200 mg, 0.512 mmol) and 3,4-bis[4-(*tert*-butyl)phenyl]-2,5-diphenylcyclopenta-2,4-dien-1-one (**6**) (636 mg, 1.28 mmol) was added 2.5 mL of *o*-Xylene. The reaction vessel was sealed and placed in a microwave reactor. Then, the mixture was stirred at 160 °C for 24 h under microwave irradiation with maximum power of 300 W. After cooling to room temperature, the resulting mixture was added to 50 mL of methanol, and the precipitates were collected via filtration, followed by purification via column chromatography over silica gel (eluent: hexane : dichloromethane = 5 : 1) to afford compound **7** (578 mg, 85% yield) as a white solid. M.p.: > 300 °C. ^{1}H NMR (500 MHz, $C_2D_2Cl_4$, 393 K, ppm) δ 7.38 – 7.23 (m, 8H), 7.17 – 7.02 (m, 11H), 6.96 – 6.88 (m, 10H), 6.87 – 6.78 (m, 8H), 6.77 –6.73 (m, 4H), 6.66 – 6.53 (m, 7H), 1.41 (s, 18H), 1.20 (s, 18H), 1.16 (s, 18H); ^{13}C NMR (125 MHz, $C_2D_2Cl_4$, 393 K, ppm) δ 148.96, 147.97, 147.63, 142.08, 141.99, 139.69, 139.63, 139.57, 139.39, 139.16, 138.73, 138.63, 138.06, 137.49, 137.19, 133.05, 132.24, 131.27,

131.09, 131.03, 129.80, 129.40, 126.85, 126.06, 125.46, 124.73, 123.93, 122.91, 122.55, 34.07, 33.76, 33.67, 31.16, 30.95, 30.91; MS (MALDI-TOF, positive) *m*/*z*: Calcd for $C_{102}H_{102}$: 1326.7982; Found: 1326.9131 $[M]^+$.

Synthesis of nanographene 1 (C78 / 27)

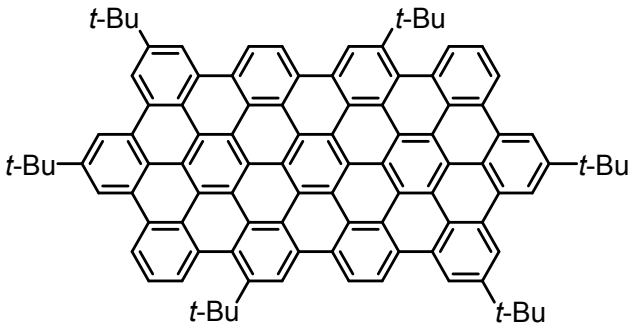

A solution of compound **7** (20.0 mg, 15.1 μmol) in unstabilized dichloromethane (35 mL) was degassed by argon bubbling for 10 min. To the degassed solution was added a suspension of iron (III) chloride (342 mg, 2.11 mmol) in nitromethane (3 mL). After stirring at room temperature for 29 h under continuous bubbling with argon pre-saturated with unstablized dichloromethane, the reaction was quenched by addition of methanol. The dark red precipitates were collected via filtration and washed intensively with methanol to afford the title compound as a dark red solid (19.2 mg, 98% yield). M.p.: > 300 °C. UV: λ_{max} = 426 nm, 521 nm, 560 nm. MS (MALDI-TOF, positive) *m*/*z*: Calcd for $C_{102}H_{74}$: 1298.5791; Found: 1298.8134 $[M]^+$. ^1H and ^{13}C NMR could not be resolved even at high temperature due to strong aggregation.

NMR spectra

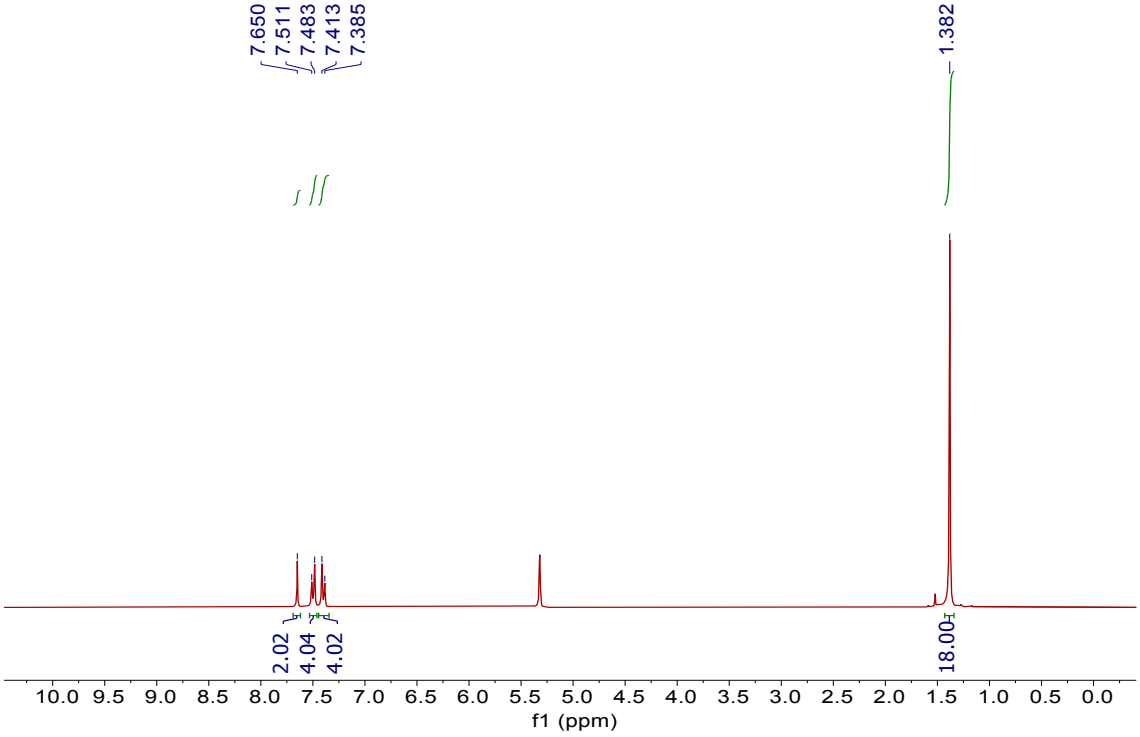

Figure S1. ^{1}H NMR spectrum of compound **3** (300 MHz, CD_2Cl_2, 298 K).

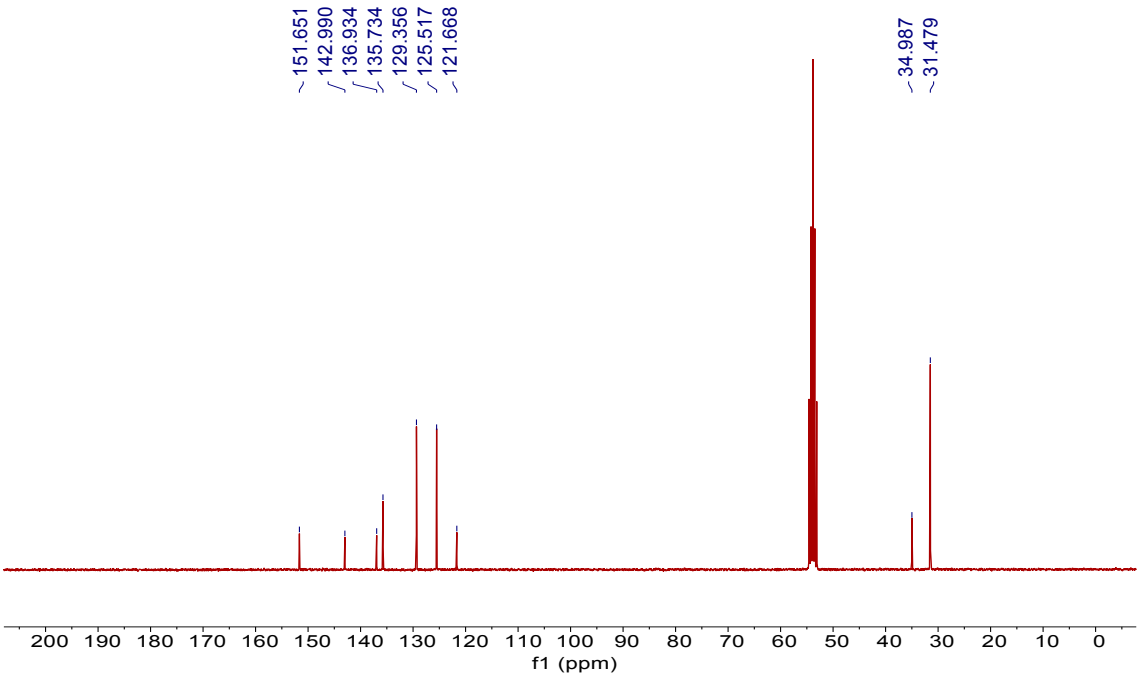

Figure S2. ^{13}C NMR spectrum of compound **3** (75 MHz, CD_2Cl_2, 298 K).

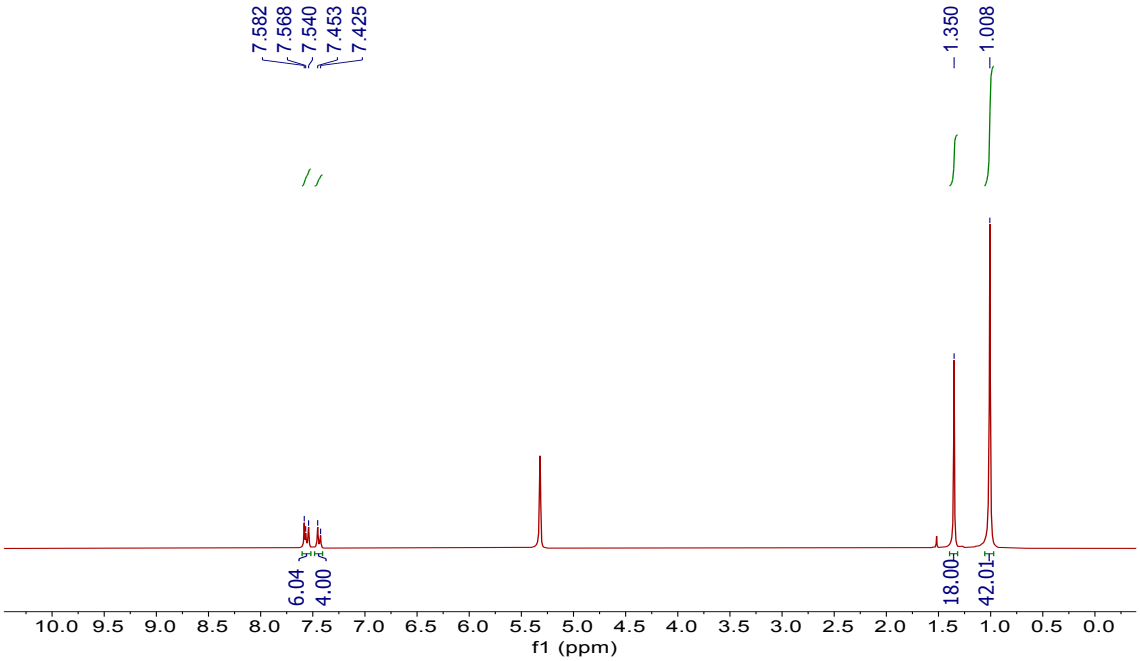

Figure S3. [1]H NMR spectrum of compound **4** (300 MHz, CD_2Cl_2, 298 K).

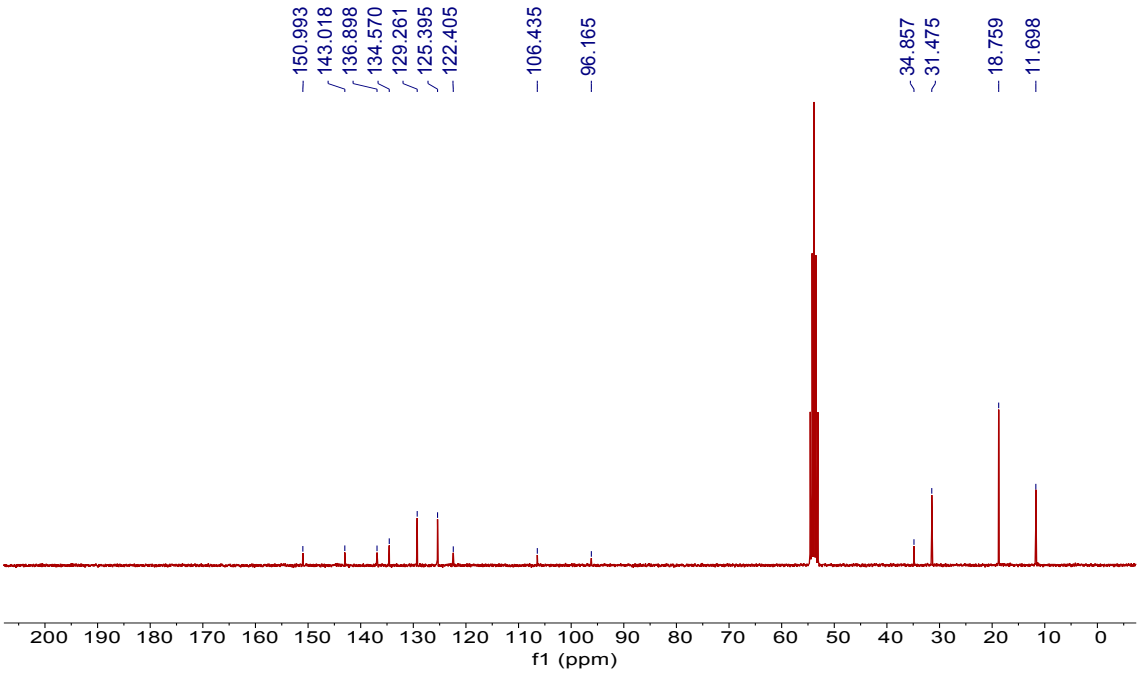

Figure S4. [13]C NMR spectrum of compound **4** (75 MHz, CD_2Cl_2, 298 K).

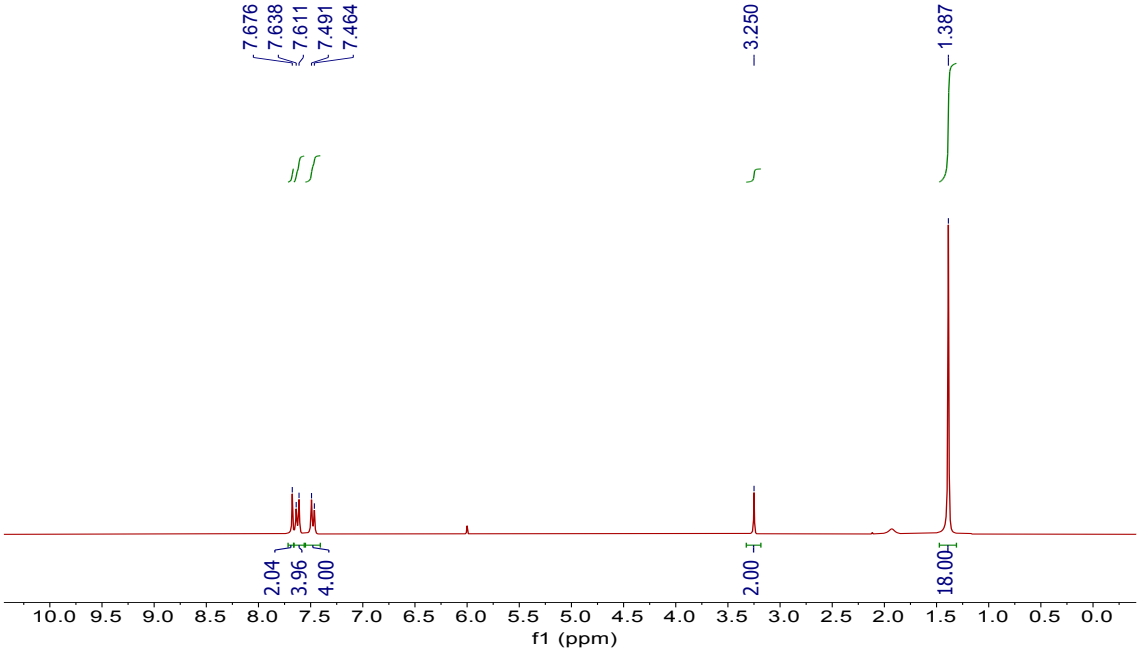

Figure S5. ^{1}H NMR spectrum of compound **5** (300 MHz, CD_2Cl_2, 298 K).

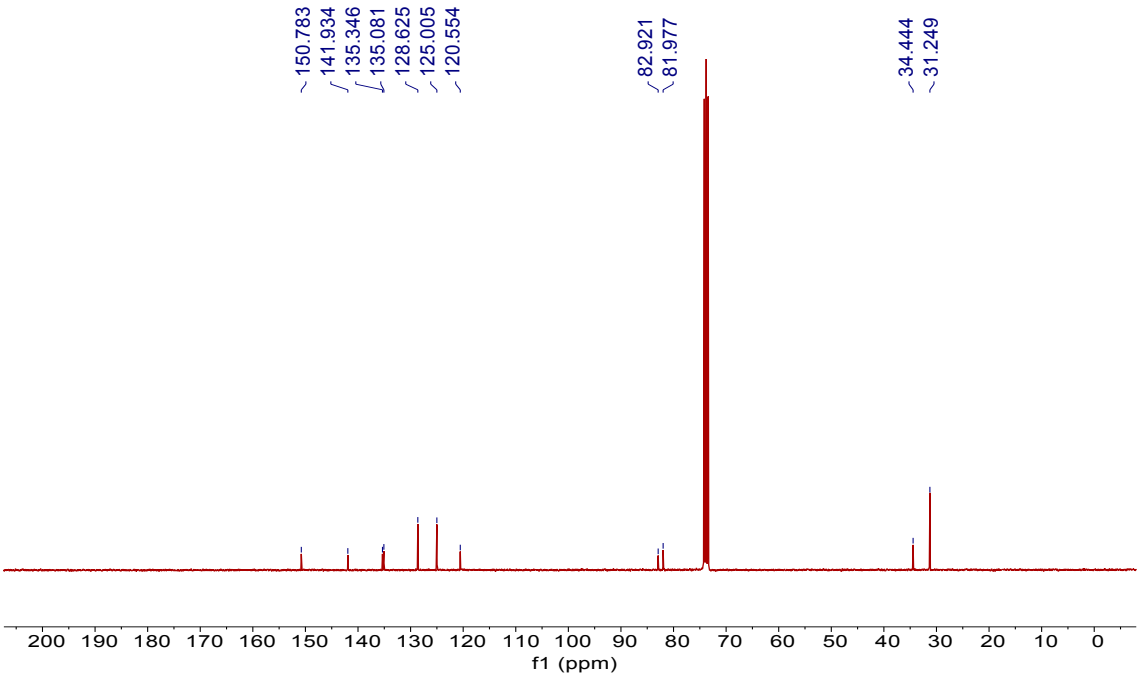

Figure S6. ^{13}C NMR spectrum of compound **5** (75 MHz, CD_2Cl_2, 298 K).

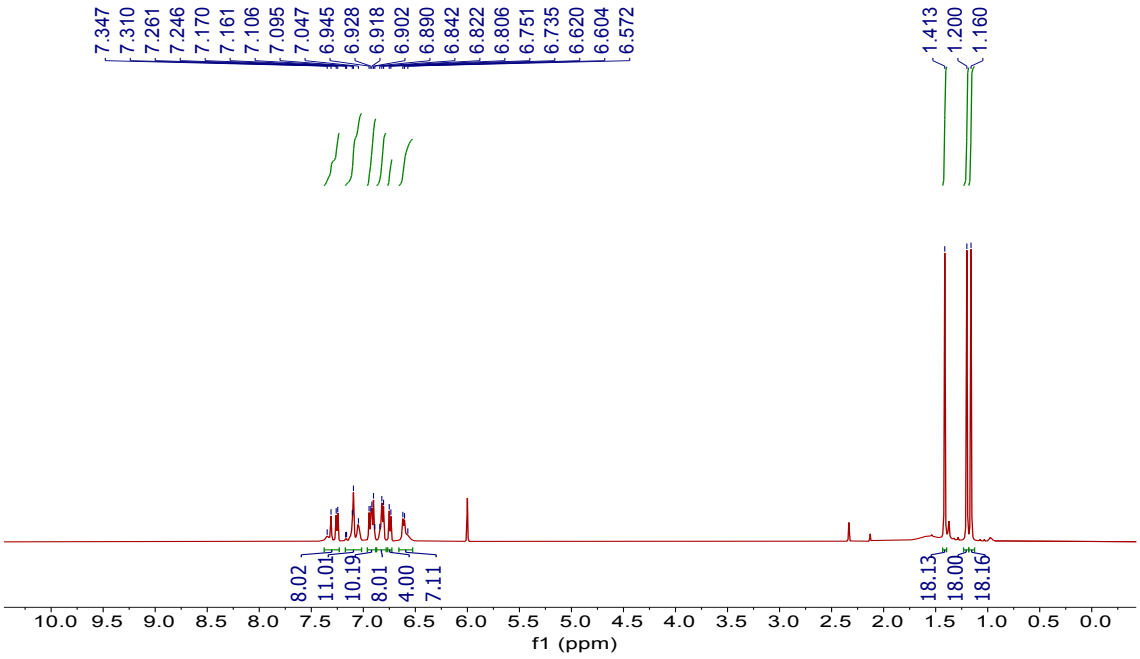

Figure S7. ^{1}H NMR spectrum of compound **7** (500 MHz, $C_2D_2Cl_4$, 393 K).

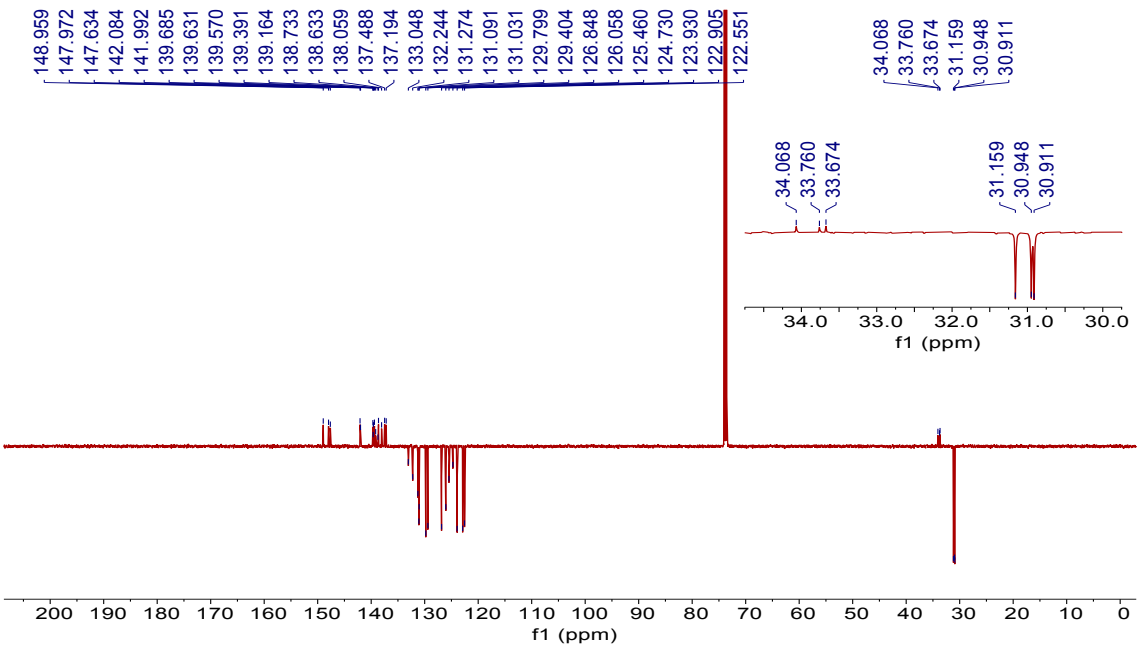

Figure S8. ^{13}C NMR spectrum of compound **7** (125 MHz, $C_2D_2Cl_4$, 393 K).

DEFINITION OF NG SIZE: PERCENTAGE OF COMPACTNESS

Many NG configurations are possible for a given number of fused rings. These can been categorized by the percentage of compactness (degree of condensation) ranging between 0% (cata-compounds) up to 100% for pure peri-condensed systems (see figure S9). The set of samples analyzed in this work are characterized by a high degree of compactness, with figures ranging between 81 and 87% (see table S1), these figures are obtained for a given number of fused rings by linear extrapolation between pure cata-condensed compounds to pure peri-condensed compounds.

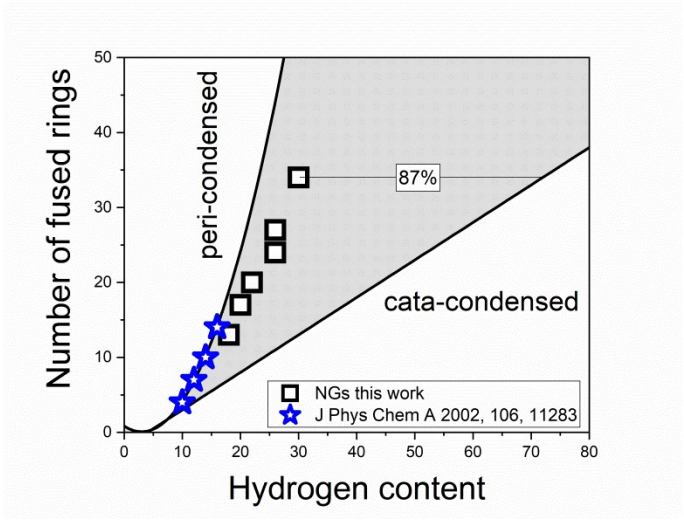

Figure S9. Number of fused rings as a function of hydrogen content for NGs with 100% compactness (blue stars) and from this work (black open squares). Adapted from J. Phys Chem A 2002, 106(46), 11283.

Table S1. HOMO-LUMO gap (ΔE_{H-L}) of NG samples analyzed in this work

	C42	C54	C60	C72	C78	C96
Compactness (%)	82	85	86	81	86	87

ABSORPTION AND EMISSION SPECTRA

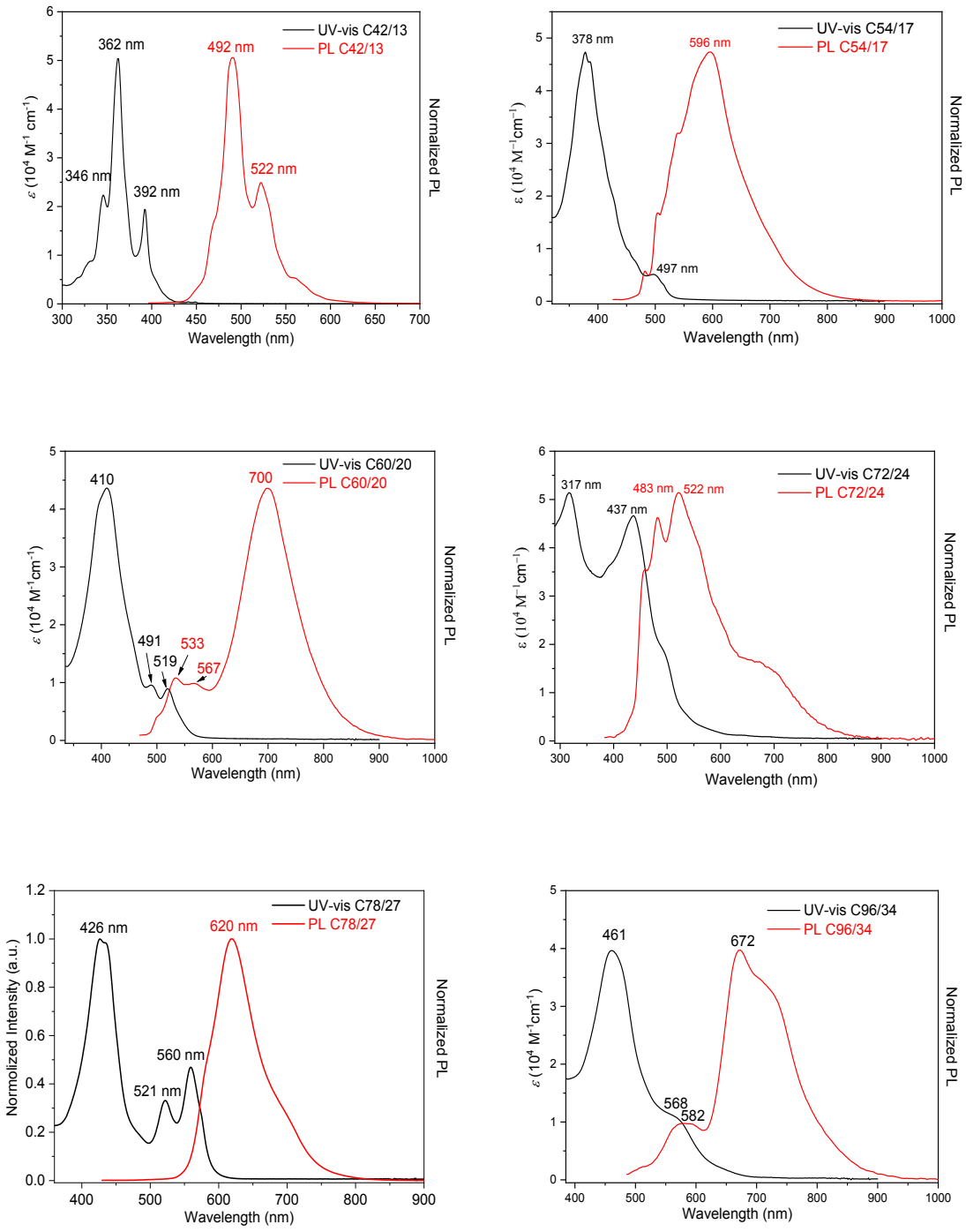

Figure S10. Absorption and Fluorescence spectrum for all analyzed set of NG samples dispersed in toluene with a concentration of 2×10^{-5} M. See details of the molecular formulae in the context of manuscript. For all analyzed NGs a strong Stokes shift is revealed while comparing their absorption and emission spectra.

For each analyzed NG sample, the difference of LUMO and HOMO levels (ΔE_{H-L}) was extracted from the onset of absorption spectrum by a linear extrapolation of the low energy band tail. A summary of all extracted results is summarized in Table S2.

Table S2. HOMO-LUMO gap (ΔE_{H-L}) of NG samples analyzed in this work

	C42	C54	C60	C72	C78	C96
ΔE_{H-L} eV	2.63	2.33	2.22	2.00	2.08	1.85

ESTIMATION OF ET DRIVING FORCE FOR THERMALIZED AND NON THERMALIZED ELECTRONS

For the slow component, we infer ΔG_{cold} conventionally as the energy onset between NG LUMO (inferred from gas phase DFT, see Fig. S11 and Table S3) and the SnO_2 CB workfunction (estimated from ultraviolet photoelectron spectroscopy spectrum of a bare SnO_2 mesoporous film as $E_{CBM} = -3.74$ eV [3]). For the fast component, ΔG_{hot} is inferred as $\Delta G_{hot} = \Delta G_{cold} + (h\nu_{pump} - \Delta E_{H-L})$ (where $h\nu_{pump}$ refers to the 400nm photon pump energy). Our estimates of ΔG_{hot} for all analyzed NG samples are listed in Table S2.

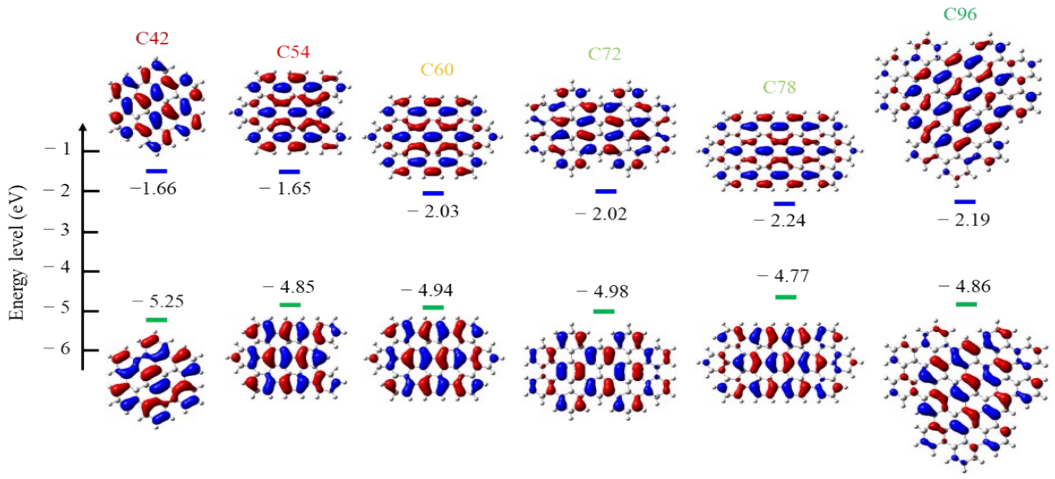

Figure S11. Workfunction and frontier orbitals for all analyzed set of NG samples calculated from DFT in the gas phase. The blue and green lines represent the LUMO and HOMO states respectively.

Table S3. Estimates for cold ET driving force (ΔG_{cold}) and hot ET driving force (ΔG_{hot}) for all analyzed NG samples.

	C42	C54	C60	C72	C78	C96
ΔG_{cold} (eV)	2.08	2.09	1.71	1.72	1.50	1.55
ΔG_{hot} (eV)	2.55	2.86	2.59	2.82	2.52	2.80

ABSORPTION FOR SENSITIZED ELECTRODES

In figure S12 (left) we show the absorbance for bare SnO_2 substrates over 400-600nm (inset reveals a broader range that enable a proper determination of SnO_2 bandgap). Several substrates revealed a featureless absorbance with a line shape that is consistent with scattering induced by the nanoparticle size distribution (black traces). However, some of the analyzed substrates revealed as well two clear below gap peaks centered at 450 and 500nm respectively. These peaks are attributed to defects populating the SnO_2 surface and have been previously linked with oxygen poor surfaces.

In figure 1(right) we present a comparison between the absorbance of NGs in solution (top panel) and the one resolved for the same NGs sensitizing SnO_2 (bottom panel). The onset of absorption for the analyzed NGs sensitizing the oxide electrode agrees well with the one obtained in solution, this can be interpreted in terms of a weak interaction at the interface, and might support the assignment of interfacial energetics conducted in this work (that is from gas phase calculations). However, it is important to note here that surface states linked with the oxide alone are likely contributing to the resolved traces. This is e.g. evident for the C42@SnO_2 trace; in any case, we do not expect that the eventual presence of surface states contributes to the interfacial ET dynamics reported here. Note that OPTP traces are only sensible to free delocalized charge carriers populating the oxide CB. Further work is needed to fully characterize the type of interaction at the NG/oxide interface, e.g. whether different oxide facets are sensitized or not; such effort is currently under scrutiny in our labs.

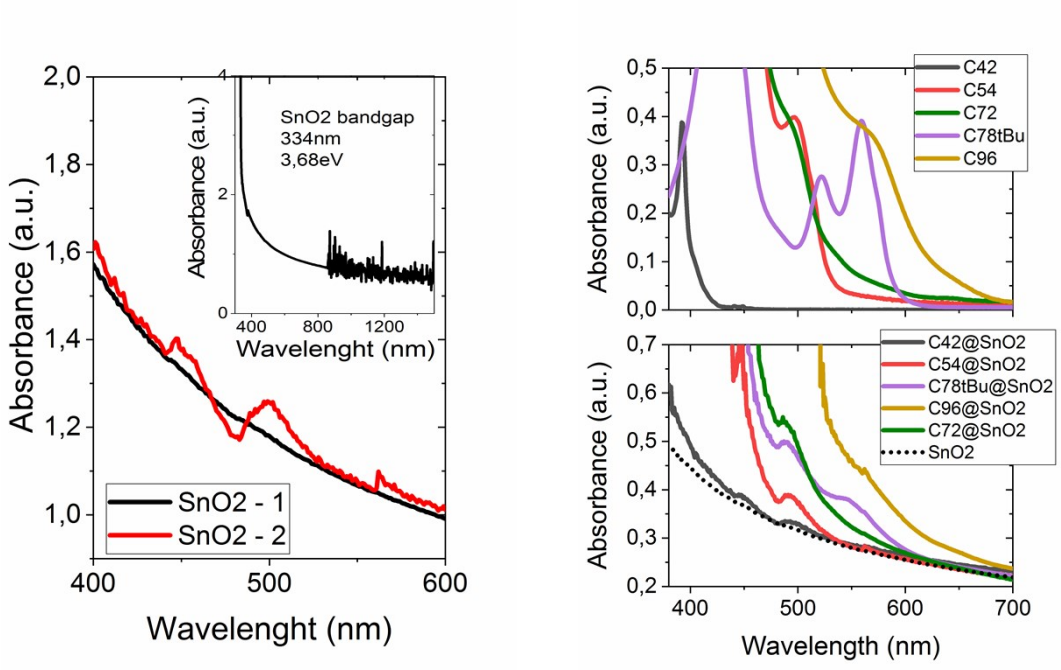

Figure S12. (Left) absorbance for bare SnO_2 substrates over 400-600nm; the inset reveals a broader range that enable a proper determination of SnO2 bandgap. (Right) comparison between the absorbance of NGs in solution (top panel) and the one resolved for the same NGs sensitizing SnO_2 (bottom panel).

References

(1) Gaussian 09, Revision D.01, Frisch, M. J.; Trucks, G. W.; Schlegel, H. B.; Scuseria, G. E.; Robb, M. A.; Cheeseman, J. R.; Scalmani, G.; Barone, V.; Mennucci, B.; Petersson, G. A.; Nakatsuji, H.; Caricato, M.; Li, X.; Hratchian, H. P.; Izmaylov, A. F.; Bloino, J.; Zheng, G.; Sonnenberg, J. L.; Hada, M.; Ehara, M.; Toyota, K.; Fukuda, R.; Hasegawa, J.; Ishida, M.; Nakajima, T.; Honda, Y.; Kitao, O.; Nakai, H.; Vreven, T.; Montgomery, Jr., J. A.; Peralta, J. E.; Ogliaro, F.; Bearpark, M.; Heyd, J. J.; Brothers, E.; Kudin, K. N.; Staroverov, V. N.; Kobayashi, R.; Normand, J.; Raghavachari, K.; Rendell, A.; Burant, J. C.; Iyengar, S. S.; Tomasi, J.; Cossi, M.;Rega, N.; Millam, N. J.; Klene, M.; Knox, J. E.; Cross, J. B.; Bakken, V.; Adamo, C.; Jaramillo, J.; Gomperts, R.; Stratmann, R. E.; Yazyev, O.; Austin, A. J.; Cammi, R.; Pomelli, C.; Ochterski, J. W.; Martin, R. L.;

Morokuma, K.; Zakrzewski, V. G.; Voth, G. A.; Salvador, P.; Dannenberg, J. J.; Dapprich, S.; Daniels, A. D.; Farkas, Ö.; Foresman, J. B.; Ortiz, J. V.; Cioslowski, J.; Fox, D. J. Gaussian, Inc., Wallingford CT, 2013.

(2) Thomas, K. R. J.; Velusamy, M.; Lin, J. T.; Chuen, C. H. and Tao, Y.-T. *J. Mater. Chem.*, 2005, **15**, 4453–4459.

(3) Han, P.; Hou, I. C.-Y.; Lu, H.; Wang, X.-Y.; Müllen, K.; Bonn, M.; Narita, A.; Cánovas, E. Chemisorption of Atomically Precise 42-Carbon Graphene Quantum Dots on Metal Oxide Films Greatly Accelerates Interfacial Electron Transfer. *J. Phys. Chem. Lett.* **2019**, 1431–1436.